Geomechanics and Engineering, *Vol. 28, No. 4 (2022) 347-358*
https://doi.org/10.12989/gae.2022.28.4.347

Fiber-reinforced micropolar thermoelastic rotating Solid with voids and two-temperature in the context of memory-dependent derivative

Amnah M. Alharbi[1a], Samia M. Said[2b], Elsayed M. Abd-Elaziz[3c] and Mohamed I.A. Othman[*2]

[1]*Department of Mathematics, College of Science, Taif Univeristy, P.O. Box 11099, Taif, 21944, Saudi Arabia*
[2]*Department of Mathematics, Faculty of Science, Zagazig University, P.O. Box 44519, Zagazig, Egypt*
[3]*Department of Basic Scineces, Zagazig Higher Institute of Eng. and Tech., Zagazig, Egypt*

(Received September 30, 2021, Revised November 23, 2021, Accepted January 9, 2022)

Abstract. The main concern of this article is to discuss the problem of a two-temperature fiber-reinforced micropolar thermoelastic medium with voids under the effect rotation, mechanical force in the context four different theories with memory-dependent derivative (MDD) and variable thermal conductivity. The three-phase-lag model (3PHL), dual-phase-lag model (DPL), Green-Naghdi theory (G-N II, G-N III), coupled theory, and the Lord-Shulman theory (L-S) are employed to solve the present problem. Analytical expressions of the physical quantities are obtained by using Laplace-Fourier transforms technique. Numerical results are shown graphically and the results obtained are analyzed. The most significant points are highlighted.

Keywords: derivative; dual-phase-lag model; Laplace and Fourier transforms; memory-dependent rotation; three-phase-lag model

1. Introduction

In geophysics, civil engineering, and aerospace structural dynamics (wings, fuselage, etc.), the role of a reinforced medium is pretty amazing. The idea of introducing continuous self-reinforcement at every point of an elastic solid was given by Belfied *et al.* (1983) utilized an elastic solid to propose the idea of employing a continuous self-reinforcement at each point. Later, Verma and Rana (1983) applied this model to a tube's rotation. In the case of a "fiber-reinforced anisotropic elastic medium", the problem of surface waves was discussed by Sengupta and Nath (2001). Roy *et al.* (2017) considered a "rotating magneto-elastic fiber-reinforced semi-space" comprising of surface stress in order to develop a better understanding of the reflection and propagation of plane waves. Othman and Said (2012) considered a 2D complexity of a thermoelastic comprising of fiber reinforcement and one relaxation time in order to understand how the rotation impacts such a medium. Sarkar and Atwa (2019) considered type II and type III Green-Naghdi theory comprising of two-temperatures, for the application of general model equations and study how the deformation of infinite isotropic space which itself is weakened by a finite linear opening mode-I crack, get influenced by the reinforcement. Othman and Said (2019) considered a thermoelastic medium facing gravity and consisting of an internal heat source to study its 2D problem of fiber reinforcement. Othman *et al.* (2014) have studied comparison of different theories on the effect of rotation on the problem of fiber-reinforced under generalized magneto-thermoelasticity subject to thermal loading due to laser pulse. Said and Othman (2015) demonstrated the influence of the mechanical force and the magnetic field on fiber-reinforced medium for the three-phase-lag model.

The behavior of these macro-molecular and granular materials can be appropriately explained with the help of the micropolar theory of elasticity. As per this theory of elasticity, the solids can not only undergo rotational and translational motions but also, may have to go through micro-rotations and macro-deformations. The non-linear theory of simple micro-elastic solid was developed by Eringen and Subhi (1964). What separates this theory of elasticity from the classical one is the fact that a micro-rotation vector (independent) is introduced in this theory. Thus, six degrees of freedom are required for the characterization of a body's motion in the micropolar theory of elasticity in which three degrees of freedom come from a rotation and the rest three from translation. Thus, in the case of a micropolar body, the transmission of interaction between two of its parts is carried out with the help of a force vector as well as a couple stress tensor and force stress tensor The micropolar theory of elasticity was developed by Eringen (1966). Parfitt and Eringen (1969) considered a micropolar elastic solid half-space and its stress-free surface to study the problem of plane waves and associated reflections. In micropolar elasticity, Marin et al. (2020), Kumar and Singh (1996), Kumar and Rani (2004), Kumar and Deswal (2001), Othman and Singh (2007), Xue

∗Corresponding author, Professor
E-mail: m_i_a_othman@yahoo.co
[a]Ph.D.
E-mail: alharbi.a.m@hotmail.com
[b]Ph.D.
E-mail: Samia_said59@yahoo.com
[c]Ph.D.
E-mail: sayed_nr@yahoo.com

ISSN: 2005-307X (Print), 2092-6219 (Online)

et al. (2010), Sarkar and Lahiri (2013), Sarkar (2014), Sarkar and Atwa (2019), Sarkar and Modal (2019), Zhang *et al.* (2015), Zhang *et al*. (2017), Barak and Kaliraman (2014), Khurana and Tomar (2019), Marin *et al*. (2013), Abbas and Marin (2018), Othman and Song (2009) investigated numerous problems based on the propagation of waves.

Said and Othman (2016) considered a "two-temperature fiber-reinforced magneto-thermoelastic medium" along with the 3PHL model to elicit details on the propagation of waves in them. Othman *et al*. (2019) too utilized the same source with the 3PHL model under the gravitational influence in order to apply the normal model analysis for the introduction of a novel model of plane waves. Despite of these several researchers working on different theories of thermoelasticity as Marin (2010), Sarkar *et al*. (2019), Sarkar and Modal (2020), Lata and Kaur (2020), Lata and Zakhmi (2019), Hobiny and Abbas (2020).

In this work, the problem is a two-temperature fiber-reinforced micropolar thermoelastic medium with voids under the influence of rotation, variable thermal conductivity, and mechanical force. The memory-dependent derivative used in instead of fractional calculus, into the four theories, the three-phase-lag model, the dual-phase- lag model, Green-Naghdi theory (GN II, GN III), coupled theory, and Lord-Shulman (L-S) theory with one relaxation time. The effect of mechanical force, magnetic field, rotation, two-temperature parameter, and kernel function on the physical quantities is presented graphically.

2. The basic equations of the problem

A problem of a two-temperature fiber-reinforced micropolar thermoelastic medium with voids in $xy-$plane with micro-rotation vector $\boldsymbol{\varphi}=(0,0,\phi_3)$. The field equations and constitutive relations can be written as Belfied *et al.* (1983) and Choudhuri (2007) in the context of generalized thermo-elasticity as follows

2.1 The stress-strain relation

$$\sigma_{ij}=\lambda e_{kk}\delta_{ij}+2\mu_T e_{ij}+\alpha(a_k a_m e_{km}\delta_{ij}+a_i a_j e_{kk})+2(\mu_L-\mu_T)(a_i a_k e_{kj} +a_j a_k e_{ki})+\beta a_k a_m e_{km} a_i a_j+\beta_1\psi\delta_{ij}-\varepsilon_{ijr}k_1\varphi_r -\gamma\theta\delta_{ij}-P(w_{ij}+\delta_{ij}), \tag{1}$$

2.2 The equations of motion

$$\rho[\ddot{u}_i+\{\boldsymbol{\Omega}\times(\boldsymbol{\Omega}\times\boldsymbol{u})\}_i+2(\boldsymbol{\Omega}\times\dot{\boldsymbol{u}})_i]=\sigma_{ji,j} \tag{2}$$

2.3 The heat conduction equation

$$K^*(1+\tau_v D_{w_3})\nabla^2\Phi+K(1+\tau_T D_{w_2})\nabla^2\Phi_{,t}=[1+\tau_q D_{w_1}+\frac{1}{2}\tau_q^2 D^2_{w_1}][\rho C_E(n_0\theta_{,tt}+n_1\theta_{,t})+\gamma T_0(n_0 e_{,tt}+n_1 e_{,t})+m n_0 T_0\psi_{,tt}+mn_1T_0\psi_{,t}]. \tag{3}$$

The relation between thermodynamic temperature θ and conductive temperature Φ is: $\Phi-\theta=\delta\Phi_{,jj}$.

2.4 The equations of void and micropolar materials

$$(\alpha_1+\beta_1+\gamma_1)\nabla(\nabla.\boldsymbol{\varphi})-\gamma_1\nabla\times(\nabla\times\boldsymbol{\varphi})+k_1(\nabla\times\boldsymbol{u})-2k_1\boldsymbol{\varphi}=\rho J\frac{\partial^2\boldsymbol{\varphi}}{\partial t^2}, \tag{4}$$

$$\alpha_2\nabla^2\psi-\alpha_3\psi-\alpha_4\frac{\partial\psi}{\partial t}-\alpha_5(\nabla.\boldsymbol{u})+m\theta=\rho\alpha_6\frac{\partial^2\psi}{\partial t^2}, \tag{5}$$

$$m_{il}=\alpha_1\varphi_{r,r}\delta_{il}+\alpha_5\varphi_{i,l}+\gamma_1\varphi_{l,i} \tag{6}$$

where $e_{ij}=\frac{1}{2}(u_{i,j}+u_{j,i})$ are the components of strain, σ_{ij} are the components of stress, λ,μ are the elastic constants, $\alpha,\beta,(\mu_L-\mu_T)$, are reinforcement parameters, α_t is the thermal expansion coefficient, ε_{ijr} is the alternate tensor, δ_{ij} is the Kronecker delta, ψ is the change in the volume fraction field, $\theta=T-T_0$, where T is the temperature above the reference temperature T_0, P is the initial stress, K^* is the additional material constant, K is the coefficient of thermal conductivity, C_E is the specific heat at constant strain, n_0,n_1 are integers, τ_T is the phase-lag of temperature gradient, τ_q is the phase-lag of heat flux, τ_v is the phase-lag of thermal displacement gradient, δ two–temperature parameter, ρ is the mass density, α_1, β_1, γ_1,k_1 are the material constants, $\alpha_2,\alpha_3,\alpha_4,\alpha_5,\alpha_6,m$ are material constants due to the presence of voids, m_{il} is the couple stress tensor, and J is microinertia. $\boldsymbol{a}\equiv(a_1,a_2,a_3)$, $a_1^2+a_2^2+a_3^2=1.$ We choose the fiber-direction as $\boldsymbol{a}\equiv(1,0,0)$. D_{wi} is the memory-dependent derivative operator is defined as Sarkar *et al.* (2019),

$$D_{w_i}f(t)=\frac{1}{w_i}\int_{t-w_i}^{t}L(t-\xi)f'(\xi)d\xi \tag{7}$$

The parameter w_i is the time-delay and $L(t-\xi)$ is the kernel function in which they can be chosen freely; see Caputo(1967), Caputo and Mainardi (1971) for more explanations.

$$L(t-\xi)=1-\frac{2b}{\varpi}(t-\xi)+a^2\frac{(t-\xi)^2}{\varpi^2} \tag{8}$$

In the present paper we take $L(t-\xi)=q+m(t-\xi)$, where q,m are constant.

To facilitate the solution, following dimensionless quantities are introduced

$$(x',y',u',v')=c_1\eta(x,y,u,v),\quad \Omega'=\frac{\Omega}{\eta c_1^2},\ (\theta',\Phi')=\frac{\gamma}{\lambda+2\mu_T}(\theta,\Phi),$$
$$(t',\tau_q',\tau_v',\tau_T')=c_1^2\eta(t,\tau_q,\tau_v,\tau_T),\ (\phi_3',\psi')=(\phi_3,\psi),$$
$$\sigma'_{ij}=\frac{\sigma_{ij}}{\lambda+2\mu_T},\quad m'_{ij}=\frac{\eta m_{ij}}{\rho c_1},\quad \eta=\frac{\rho C_E}{K^*},\quad c_1^2=\frac{\lambda+2\mu_T}{\rho}. \tag{9}$$

Using Kirchhoff transformation (Noda 1986)

$$K=K(\theta)=K_0(1+K_1\theta),\quad K=K(\Phi)=K_0(1+K_1\Phi). \tag{10}$$

Where K_0 is a constant which is equal to the thermal conductivity of the material when it does not depend on the thermodynamic temperature (θ) and K_i is a non-positive small parameter.

Using new functions ψ_1, ψ_2 to express heat conduction in the Kirchhoff transformation (Noda 1986)

$$\psi_1 = \frac{1}{K_0}\int_0^{\Phi} K(\Phi')\,d\Phi', \qquad \psi_2 = \frac{1}{K_0}\int_0^{\theta} K(\theta')\,d\theta'. \tag{11}$$

Using Eqs. (10) and (11), we get

$$\psi_1 = \Phi(1+\frac{K_1}{2}\Phi), \qquad \psi_2 = \theta(1+\frac{K_1}{2}\theta). \tag{12}$$

For linearity, then the above equation will be reduced to

$$\frac{\partial \Phi}{\partial x_i} = \frac{\partial \psi_1}{\partial x_i}, \qquad \frac{\partial \theta}{\partial x_i} = \frac{\partial \psi_2}{\partial x_i}. \tag{13}$$

Using the above Eqs. (2)-(5), we get

$$\frac{\partial^2 u}{\partial t^2} - \Omega^2 u - 2\Omega \dot{v} = B_1\frac{\partial^2 u}{\partial x^2} + B_2\frac{\partial^2 v}{\partial x\,\partial y} + B_3\frac{\partial^2 u}{\partial y^2} + B_4\frac{\partial \psi}{\partial x} + B_5\frac{\partial \phi_3}{\partial y} - \frac{\partial \psi_2}{\partial x}, \tag{14}$$

$$\frac{\partial^2 v}{\partial t^2} - \Omega^2 v + 2\Omega \dot{u} = B_3\frac{\partial^2 v}{\partial x^2} + B_2\frac{\partial^2 u}{\partial x\,\partial y} + B_6\frac{\partial^2 v}{\partial y^2} + B_4\frac{\partial \psi}{\partial y} - B_5\frac{\partial \phi_3}{\partial x} - \frac{\partial \psi_2}{\partial y}, \tag{15}$$

$$(1+\tau_v D_{w_3})\psi_{1,ii} + B_7(1+\tau_T D_{w_2})\psi_{1,iit} = [1+\tau_q D_{w_1} + \frac{1}{2}\tau_q^2 D_{w_1}^2][B_8\psi_{2,tt} + B_9\dot{\psi}_2 + B_{10}e_{,tt} + B_{11}e_{,t} + B_{12}\psi_{,tt} + B_{13}\psi_{,t}], \tag{16}$$

$$\nabla^2\phi_3 + B_{14}(\frac{\partial_v}{\partial_x} - \frac{\partial_u}{\partial_y}) - B_{15}\phi_3 = B_{16}\frac{\partial^2 \phi_3}{\partial t^2}, \tag{17}$$

$$\nabla^2\psi - B_{17}\psi - B_{18}\frac{\partial \psi}{\partial t} - B_{19}(\frac{\partial u}{\partial x} + \frac{\partial v}{\partial y}) + B_{20}\psi_2 = B_{21}\frac{\partial^2 \psi}{\partial t^2}, \tag{18}$$

where B_i's are given in the appendix.

3. The analytical solution of the problem

The problem is solved using the Laplace and Fourier transform defined by

$$\bar{f}(x,y,s) = \int_0^{\infty} f(x,y,t)\,e^{-st}dt, \tag{19}$$

$$f^*(\zeta,y,s) = \int_{-\infty}^{\infty} \bar{f}(x,y,s)\,e^{i\zeta x}dx. \tag{20}$$

Introducing Eqs. (19) and (20) in Eqs. (14)-(18), thus we get

$$(B_3 D^2 - N_1)u^* + (i\zeta B_2 D + 2\Omega s)v^* - i\zeta(N_{11} - N_{12}D^2)\psi_1^* + i\zeta B_4\psi^* + B_5 D\phi_3^* = 0, \tag{21}$$

$$(i\zeta B_2 D - 2\Omega s)u^* + (B_6 D^2 - N_2)v^* - D(N_{11} - N_{12}D^2)\psi_1^* + B_4 D\psi^* - i\zeta B_5\phi_3^* = 0, \tag{22}$$

$$-B_{14}Du^* + i\zeta B_{14}v^* + (D^2 - N_3)\phi_3^* = 0, \tag{23}$$

$$-i\zeta B_{19}u^* - B_{19}Dv^* + B_{20}(N_{11} - N_{12}D^2)\psi_1^* + (D^2 - N_4)\psi^* = 0, \tag{24}$$

$$N_9 u^* + N_8 Dv^* + (N_{13} - N_{14}D^2)\psi_1^* + N_{10}\psi^* = 0, \tag{25}$$

where N_i's are given in the Appendix and $D = \frac{d}{dy}$.

The system of Eqs. (21)-(25) are solved to obtain

$$(D^{10} - E_1 D^8 + E_2 D^6 - E_3 D^4 + E_4 D^2 - E_5)u^*(y) = 0 \tag{26}$$

where E_i's are given in the appendix.

The solution of Eq. (26) bound as $y \to \infty$, is given by

$$u^*(y) = \sum_{n=1}^{3} J_n \exp(-I_n y). \tag{27}$$

In similar manner, we get

$$\phi_3^*(y) = \sum_{n=1}^{3} J_n H_{1n} \exp(-I_n y), \tag{28}$$

$$v^*(y) = \sum_{n=1}^{3} J_n H_{2n} \exp(-I_n y), \tag{29}$$

$$\psi_1^*(y) = \sum_{n=1}^{3} J_n H_{3n} \exp(-I_n y), \tag{30}$$

$$\psi^*(y) = \sum_{n=1}^{3} J_n H_{4n} \exp(-I_n y), \tag{31}$$

$$\psi_2^*(y) = \sum_{n=1}^{3} J_n H_{5n} \exp(-I_n y). \tag{32}$$

Using Eqs. (9), (19, 20), (27)- (32) in Eqs. (1) and (6), we get

$$\sigma_{yy}^*(y) = \sum_{n=1}^{3} J_n H_{6n} \exp(-I_n z), \tag{33}$$

$$\sigma_{xy}^*(y) = \sum_{n=1}^{3} J_n H_{7n} \exp(-I_n y), \tag{34}$$

$$m_{yz}^*(y) = \sum_{n=1}^{3} J_n H_{8n} \exp(-I_n z). \tag{35}$$

Where H_{in}'s are given in the Appendix.

4. Boundary condition

In the physical problem, we should suppress the positive exponentials that are unbounded at infinity. The constants I_1, I_2, I_3, I_4, I_5 have to chosen such that the boundary conditions on the surface at $y = 0$ take the form

$$\sigma_{yy} = -P_1\delta(x)F(t),\ \sigma_{xy} = 0,\ m_{yz} = 0,$$
$$\psi_2 = P_2\delta(x)F(t),\ \frac{\partial \psi}{\partial y} = P_3\delta(x)F(t). \tag{36}$$

Where P_1, P_2, P_3 are the magnitudes of mechanical force, thermal source and volume source respectively. $\delta(x)$ is the Dirac-delta function and in this paper, we consider two types of loads on the plane boundary for which is as defined below

$$F(t) = \begin{cases} H(t) & \text{for continuous load} \\ \delta(t) & \text{for impact load} \end{cases} \tag{37}$$

4.1 Continuous load

Substituting Eqs. (31)-(35) in Eqs. (36), we can obtain the following equations satisfied with the parameters

$$\sum_{n=1}^{5} H_{4n} J_n I_n = -\frac{P_3}{s}, \quad \sum_{n=1}^{5} H_{5n} J_n = \frac{P_2}{s}, \quad \sum_{n=1}^{5} H_{6n} J_n = -\frac{P_1}{s}, \quad \sum_{n=1}^{5} H_{7n} J_n = 0, \quad \sum_{n=1}^{5} H_{8n} J_n = 0. \tag{38}$$

After applying the inverse of the matrix method, we have

$$\begin{pmatrix} J_1 \\ J_2 \\ J_3 \\ J_4 \\ J_5 \end{pmatrix} = \begin{pmatrix} I_1 H_{41} & I_2 H_{42} & I_3 H_{43} & I_4 H_{44} & I_5 H_{45} \\ H_{51} & H_{52} & H_{53} & H_{54} & H_{55} \\ H_{61} & H_{62} & H_{63} & H_{64} & H_{65} \\ H_{71} & H_{72} & H_{73} & H_{74} & H_{75} \\ H_{81} & H_{82} & H_{83} & H_{84} & H_{85} \end{pmatrix}^{-1} \begin{pmatrix} -P_3/s \\ P_2/s \\ -P_1/s \\ 0 \\ 0 \end{pmatrix}. \tag{39}$$

4.2 Impact load

We can obtain the following equations satisfied with the parameters

$$\sum_{n=1}^{5} H_{4n} J_n I_n = -P_3, \ \sum_{n=1}^{5} H_{5n} J_n = P_2, \ \sum_{n=1}^{5} H_{6n} J_n = -P_1, \ \sum_{n=1}^{5} H_{7n} J_n = 0, \ \sum_{n=1}^{5} H_{8n} J_n = 0, \tag{40}$$

After applying the inverse of the matrix method, we have

$$\begin{pmatrix} J_1 \\ J_2 \\ J_3 \\ J_4 \\ J_5 \end{pmatrix} = \begin{pmatrix} I_1 H_{41} & I_2 H_{42} & I_3 H_{43} & I_4 H_{44} & I_5 H_{45} \\ H_{51} & H_{52} & H_{53} & H_{54} & H_{55} \\ H_{61} & H_{62} & H_{63} & H_{64} & H_{65} \\ H_{71} & H_{72} & H_{73} & H_{74} & H_{75} \\ H_{81} & H_{82} & H_{83} & H_{84} & H_{85} \end{pmatrix}^{-1} \begin{pmatrix} -P_3 \\ P_2 \\ -P_1 \\ 0 \\ 0 \end{pmatrix}. \tag{41}$$

After obtaining ψ_1, ψ_2 the conductive temperature and the thermodynamic temperature can be obtained by solving Eq. (12) to give

$$\theta = \frac{-1+\sqrt{1+2K_1\psi_2}}{K_1}, \qquad \Phi = \frac{-1+\sqrt{1+2K_1\psi_1}}{K_1}. \tag{41}$$

5. Special cases

5.1 If P_1=1, P_2=0, P_3=0, we obtain the corresponding expressions for normal force applied on the plane surface.

5.2 If P_1=0, P_2=1, P_3=0, then the corresponding expressions yield the results for thermal sources.

5.3 If P_1=0, P_2=0, P_3=1, then the corresponding expressions are obtained for volume fraction field sources.

6. Inversion of The transforms

The transformed displacements, thermodynamic temperature, the conductive temperature, the stress components, the change in the volume fraction and the tangential couple stress are the functions of y and the parameters s and ζ of Laplace and Fourier transforms respectively and hence are of the form $f^*(\zeta, y, s)$. To obtain the solution of the problem in the physical domain, we invert the Laplace and Fourier transforms by using the method described by Kumar and Rani (2004).

7. Numerical calculations and discussion

To study the influence of a magnetic field and gravity on wave propagation, we use the following physical constants for generalized fiber-reinforced micropolar thermoelastic materials (Said and Othman 2020)

$\lambda = 5.65\times10^{10}\,\text{N.m}^{-2}$, $\mu_T = 2.46\times10^{10}\,\text{N.m}^{-2}$, $T_0 = 293\text{K}$, $\mu_L = 5.66\times10^{10}\,\text{N.m}^{-2}$, $\beta_1 = 2.68\times10^{6}\,\text{N.m}^{-2}$, $\rho = 2660\text{kg.m}^{-3}$, $\beta = 0.015\times10^{-4}\,\text{N.m}^{-2}$, $\omega_2 = 0.06$, $\gamma_1 = 0.779\times10^{-8}\,\text{N.m}^{-2}$, $\alpha_1 = 1.28\times10^{10}\,\text{N.m}^{-2}$, $\alpha_t = 1.78\times10^{-4}\,\text{K}^{-1}$, $k_1 = 85\,\text{dyne/m}^2$, $C_E = 0.787\times10^{3}\,\text{kg.K}^{-1}$, $K^* = 150\,\text{w.m}^{-1}\text{.K}^{-1}$, $\omega_3 = 0.07$, $\omega_1 = 0.04$, $t = 0.02$, $x = 0.2$, $n = 0.5$, $q = 0.3$, $\beta_1 = 0.07$, $\tau_q = 0.7$, $\tau_T = 0.5$, $\tau_\upsilon = 0.3$, $K_1 = -0.8$, $0 \le y \le 20$.

The void parameters are taken as (Othman and Said 2019)

$\alpha_2 = 3.668\times10^{-5}\text{dyne}$, $\alpha_3 = 1.475\times10^{10}\text{dyne/cm}^2$, $\alpha_4 = 0.0787\times10^{-3}\,\text{dyne.sec/cm}^2$, $m = 2\times10^{6}\,\text{N/m}^2\text{K}$, $\alpha_5 = 1.13849\times10^{10}\text{dyne/cm}^2$, $\alpha_6 = 1.753\times10^{-15}\text{dyne/cm}^2$.

The comparisons have been made in the context of three theories of thermoelasticity, namely; (3PHL), (G-N: III)) and (L-S), in four situations:

(i) Two values for rotation parameter ($\Omega = 0.2, \Omega = 0.4$).

(ii) Whether we have one temperature or two temperature ($\delta = 0.8$ and $\delta = 0$).

(iii) With and without initial stress (p=100 and p=0).

(iv) Two types of mechanical loads (continuous load and impact load).

(v) Effect of thermal conductivity (K_1= -0.8, K_1 = -1.2).

7.1 The effect of rotation

Figs. 1-5 show the variations of the non-dimensional thermodynamic temperature θ, the stress component. σ_{xy}, the couple stress tensor component m_{yz}, the change in the volume fraction field ψ and the Micro rotation component ϕ_3, respectively, for two different values of rotation parameter $\Omega(\Omega = 0.2, 0.4)$, $\delta = 0.8$, p=100, K_1=0.08.

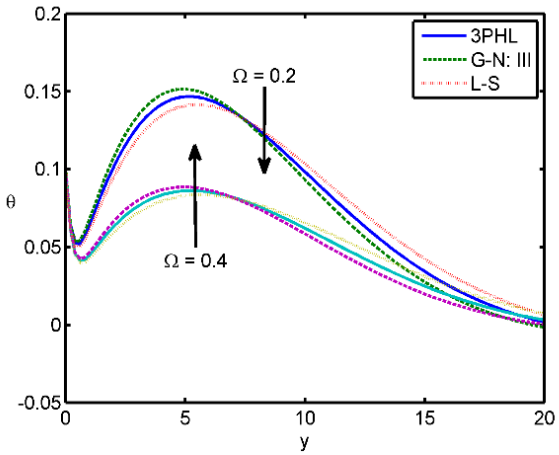

Fig. 1 The variation of thermodynamic temperature θ for different theories at two values of rotation

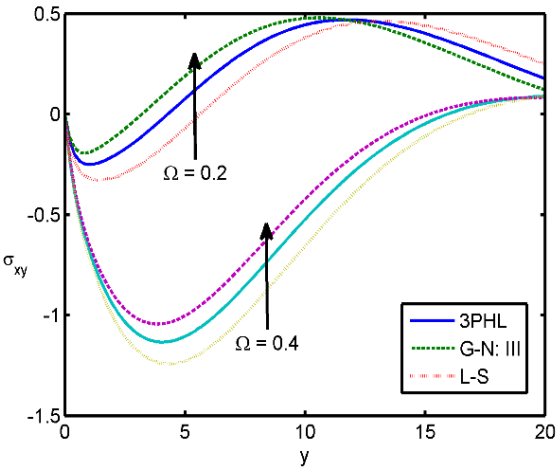

Fig. 2 The variation of stress component σ_{xy} for different theories at two values of rotation

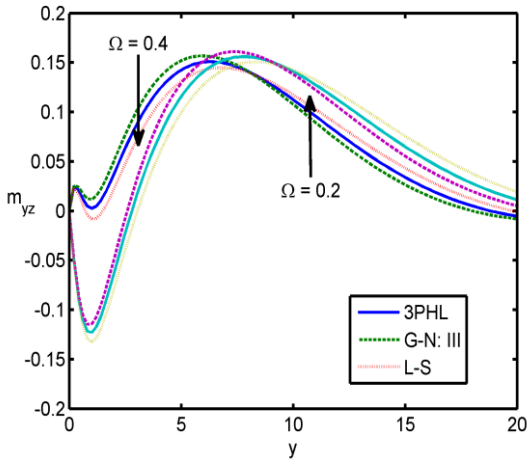

Fig. 3 The variation of the couple stress tensor component m_{yz} for different theories at two values of rotation

In each graph, there are six curves predicted by the three models 3PHL, G-N: III, and L-S, considered in this work.

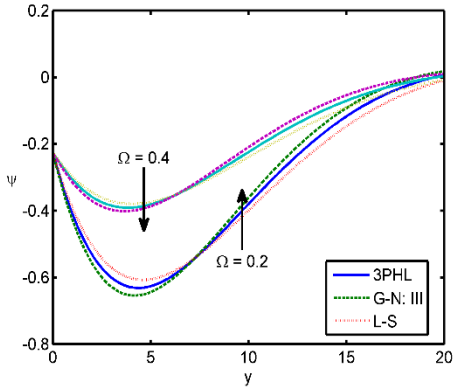

Fig. 4 The variation of the change in the volume fraction field ψ for different theories at two values of rotation

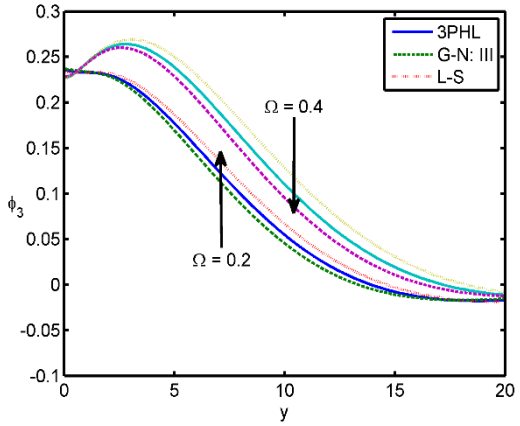

Fig. 5 The variation of the microrotation component ϕ_3 for different theories at two values of rotation

In these figures, the solid lines represent the solution in the 3PHL model, the dashed lines represent the solution derived using the G-N III theory and the dot lines represent the solution in L-S theory. Here all the variables are taken in non-dimensional forms. We noticed that, the rotation parameter has a significant effect on all fields. Fig. 1 investigated the variation of thermodynamic temperature θ, with distance y in this figure, the magnitude of the thermodynamic temperature and the conductive temperature are decreasing with decreasing the value of rotation parameter. Fig. 2 displays the variation of the stress component σ_{xy}, against the distance y. We noticed that the stress components have been affected by the rotation, where the increasing of rotation parameter causes a decreasing in value of σ_{xy}. These figures also show that the boundary conditions are identically satisfied by the stress components. Figs. 3-5 illustrate the variation of the couple stress tensor component m_{yz}, the change in the volume fraction field ψ and the Micro rotation component ϕ_3 versus y. It is also manifested from the figures that increase values of rotation are having an increase effect on the magnitude of m_{yz}, ψ and ϕ_3.

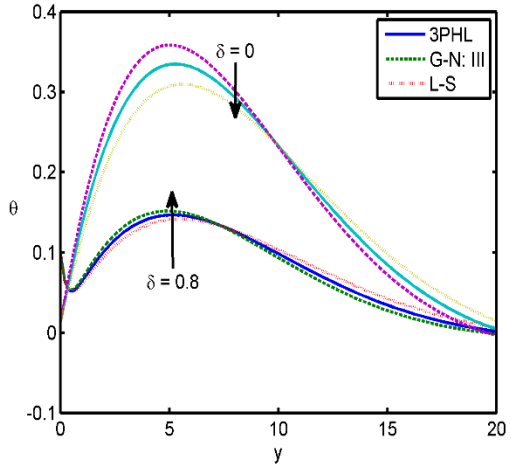

Fig. 6 The variation of thermodynamic temperature θ for different theories at two values of two temperature parameter

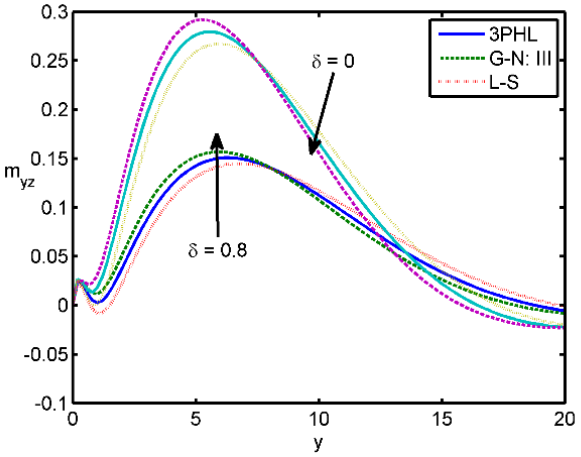

Fig. 8 The variation of the couple stress tensor componen m_{yz} for different theories at two values of two temperature parameter

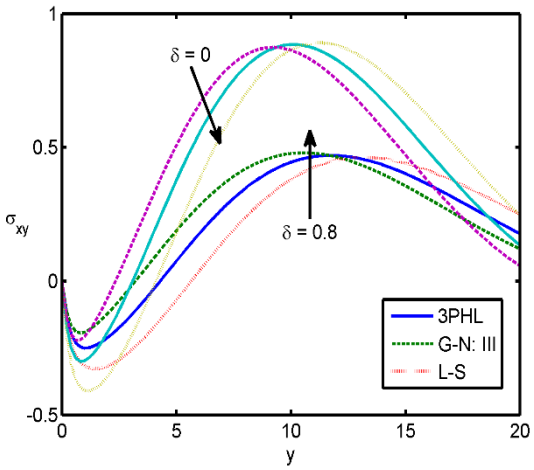

Fig. 7 The variation of stress component σ_{xy} for different theories at two values of two temperature parameter

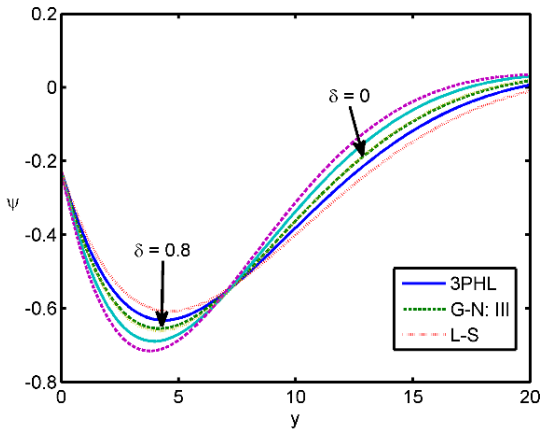

Fig. 9 The variation of the change in the volume fraction field ψ for different theories at two values of two temperature parameter

7.2 One temperature or two temperatures

Figs. 6-10 show the variations of the non-dimensional thermodynamic temperature θ, the stress component σ_{xy}, the couple stress tensor component m_{yz}, the change in the volume fraction field ψ and the micro-rotation component ϕ_3, respectively, for one temperature $(\delta = 0)$ and two temperatures $(\delta = 0.8)$ at $\Omega = 0.2,\ p = 100,\ K_1 = -0.8$. Fig. 6 explains that the distribution of thermodynamic temperature θ, begins from positive values. In the context of three theories, the values of the thermodynamic temperature θ, for two temperatures are large compared to those for one temperature in the range $0 \le y \le 1$; small in the range $1 \le y \le 20$, while the values are the same for two cases at $y \ge 20$. Fig. 7 exhibits the distribution of the stress component σ_{xy} and demonstrates that it reaches a zero value and satisfies the boundary condition at $y = 0$. In the context of the three theories, the two temperature parameter decrease the magnitudes of σ_{xy}. Fig. 8 depicts the distribution of the couple stress tensor component m_{yz} and demonstrates that it reaches a zero value and satisfies the boundary condition at $y = 0$. By comparing two solution curves it is found that absolute values of m_{yz} are smaller in the presence of two temperature parameter. Fig. 9 shows the distribution of the change in the volume fraction field ψ, the values of ψ for two temperatures are large compared to those for one temperature in the range $0 \le y \le 7$; small in the range $7 \le y \le 20$, while the values are the same for two cases at $y \ge 20$. ig. 10 has been plotted to observe the effect of two temperatures parameter on the micro-rotation component ϕ_3 against distance y For both cases, the amplitude distribution of ϕ_3 decreases owing to increasing values of two-temperature discrepancy.

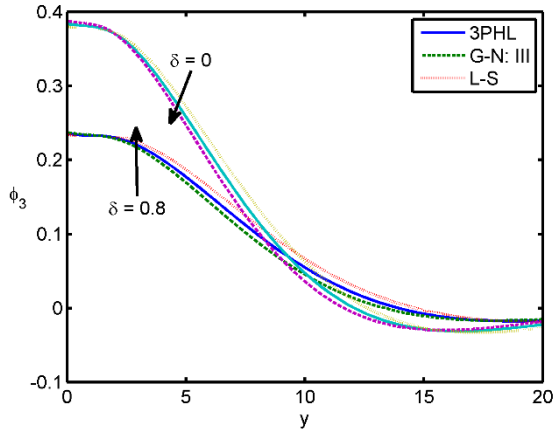

Fig. 10 The variation of the microrotation component ϕ_3 for different theories at two values of two temperature parameter

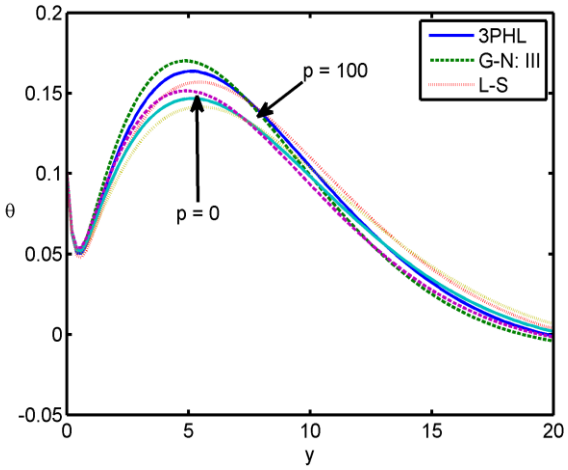

Fig. 11 The variation of thermodynamic temperature θ for different theories at two values of initial stress parameter

7.3 Effect of initial stress

Figs. 11-15 show the variations of the non-dimensional thermodynamic temperature θ, the stress component σ_{xy}, the couple stress tensor component m_{yz}, the change in the volume fraction field ψ and the micro-rotation component ϕ_3, respectively, with and without initial stress (p =100 and p =0). The initial stress parameter has a significant role in the distribution of all physical quantities in the problem. Fig. 11 shows the distribution of the thermo-dynamic temperature θ versus the distance y. The values of the temperature θ for presence initial stress are large compared to those for absence initial stress in the range $0 \le y \le 20$, while the same values at $y \ge 20$. Fig. 12 shows the distribution of the stress component σ_{xy} versus the distance y. It is found that, the magnitude of the stress component σ_{xy} increases with the increase of the parameter of initial stress. Fig. 13 shows the distribution of

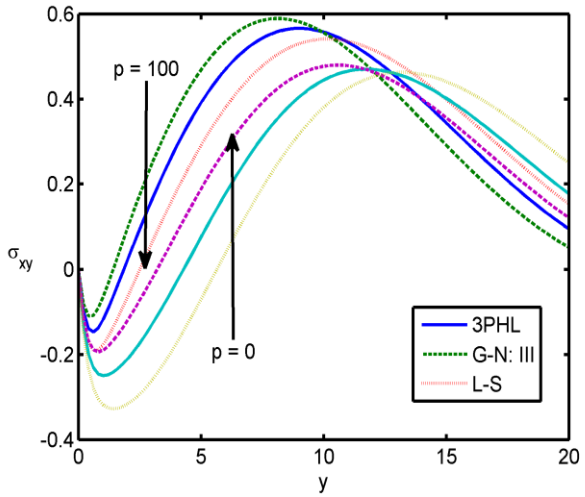

Fig. 12 The variation of stress component σ_{xy} for different theories at two values of initial stress parameter

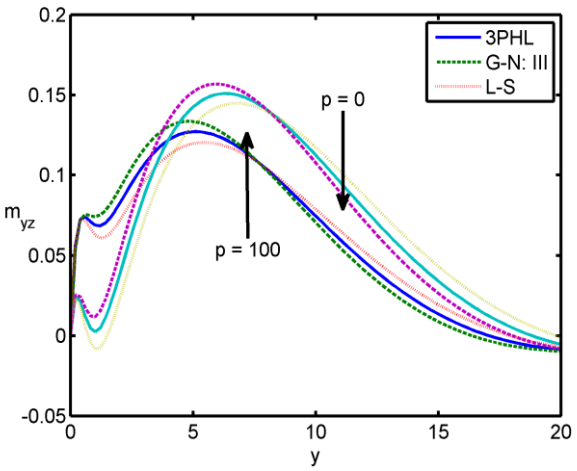

Fig. 13 The variation of the couple stress tensor component m_{yz} for different theories at two values of initial stress parameter

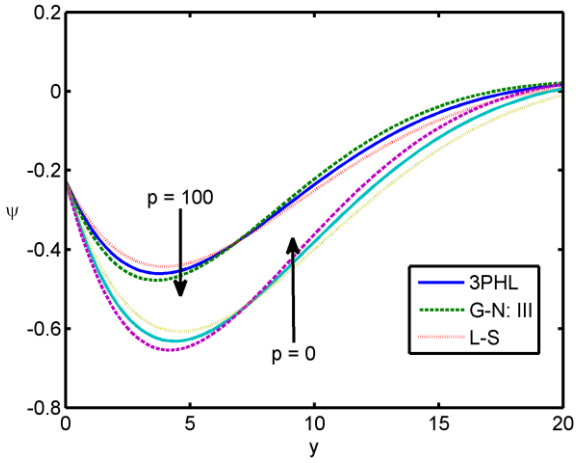

Fig. 14 The variation of the change in the volume fraction field ψ for different theories at two values of initial stress parameter

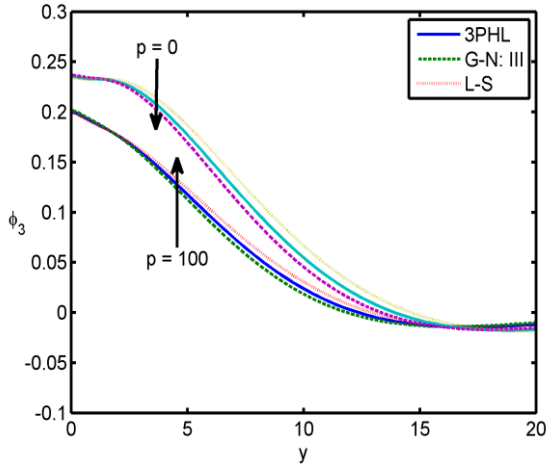

Fig. 15 The variation of the microrotation component ϕ_3 for different theories at two values of initial stress parameter

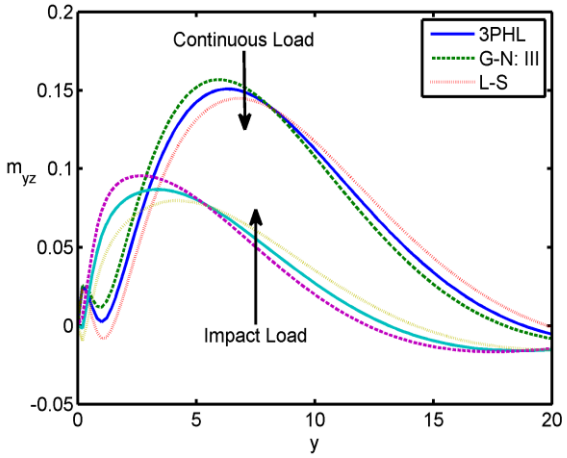

Fig. 17 The variation of the couple stress tensor component m_{yz} for different theories at two kinds of mechanical loads

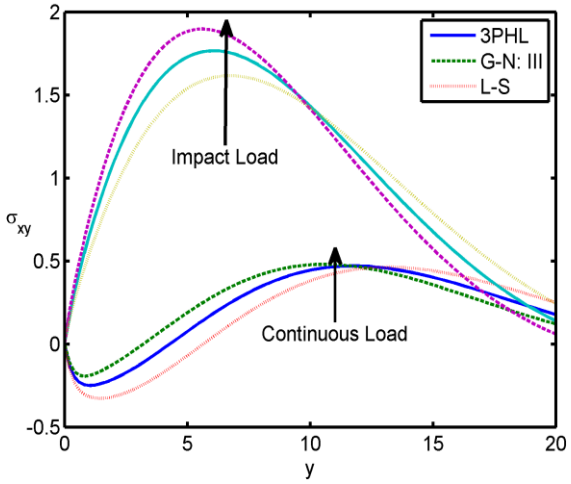

Fig. 16 The variation of the stress component σ_{xy} for different theories at two kinds of mechanical loads

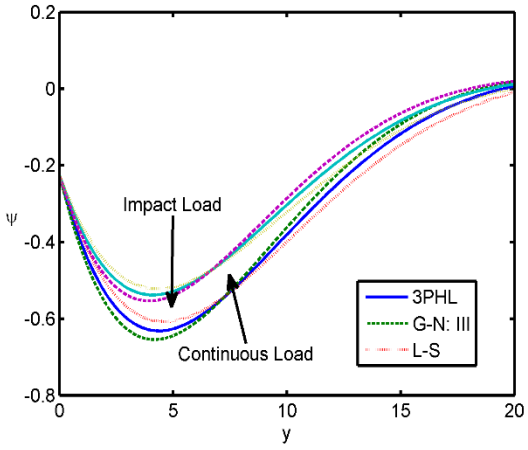

Fig. 18 The variation of the change in the volume fraction field ψ for different theories at two kinds of mechanical loads of initial stress parameter

the couple stress tensor component m_{yz}. It can be seen that the magnitude of m_{yz} is found to be large for the presence of initial stress in the range $0 \le y \le 4$; small in the range $4 \le y \le 20$, while the values are the same for two cases at $y \ge 20$. Fig. 14 indicates the distribution of the change in the volume fraction field ψ. It is clear that, the initial stress acts to increase the magnitude of the change in the volume fraction field. Fig. 15 shows the distribution of the Micro rotation component ϕ_3 against distance y. For both cases, the initial stress acts to decrease the magnitude of the micro-rotation component.

7.4 The influence of the mechanical loads

Figs. 16-19 show the variations of the physical quantities, which demonstrate the effects of the mechanical loads (continuous load and impact load) on the variations of the considered variables when $p_1 = p_2 = p_3 = 0.1$, at $\delta = 0.8, \Omega = 0.2, p = 100, K_1 = -0.8$. These figures evidence that, the behavior of all models may be the same with different amplitudes. Fig. 16 indicates the variation of the stress component σ_{xy} versus y. In this figure, the impact load increases the values of stress component σ_{xy}, also, it is observed that: in the context of the three theories, the values of the tangential stress component σ_{xy} start from a zero, which satisfy the boundary conditions. Fig. 17 studies the variation of the couple stress tensor component m_{yz}. It is observed that: the values of m_{yz} for the continuous load are large compared to those for the impact load in the range $0 \le y \le 1$; small in the range $1 \le y \le 3$; large in the range $3 \le y \le 20$; while the values are the same for two cases at $y \ge 20$. Fig. 18 investigates the variation of the change in the volume fraction field ψ against distance y.

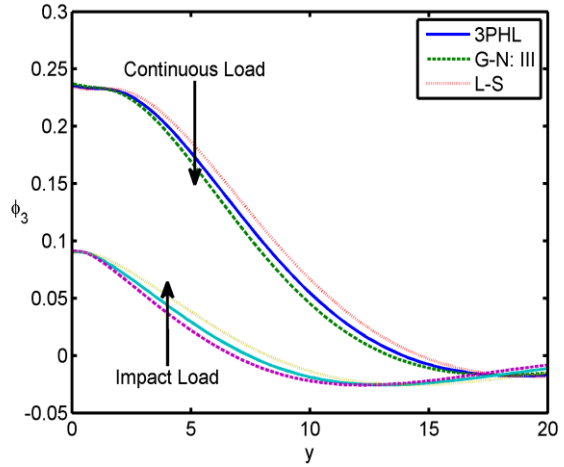

Fig. 19 The variation of the microrotation component ϕ_3 for different theories at two kinds of mechanical loads

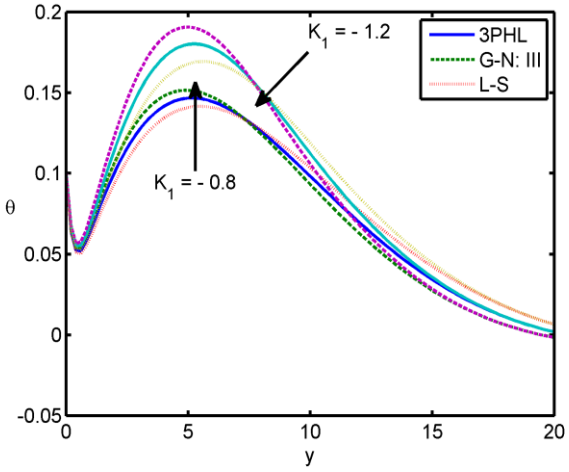

Fig. 20 The variation of thermodynamic temperature θ for different theories at two values of thermal conductivity parameter.

In this figure, the impact load increases the values of ψ. Fig. 19 shows the distribution of the micro-rotation component ϕ_3 against distance y. It is found that, the values of ϕ_3 for the continuous load are large compared to those for the impact load in the range $0 \le y \le 17$, while the values are the same for two cases at $y \ge 17$.

7.5 Effect of thermal conductivity

Figs. 20-23 display the variations of the non-dimensional thermodynamic temperature θ, the couple stress tensor component m_{yz}, the change in the volume fraction field ψ and the microrotation component ϕ_3, respectively, for different values of the thermal conductivity ($K_1 = -0.5$ and $K_1 = -1$), i.e. this study considers that thermal conductivity depends on the temperature. Figs. 22

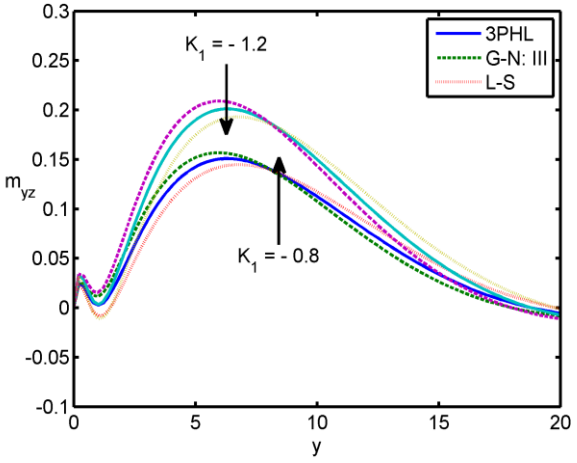

Fig. 21 The variation of the couple stress tensor component m_{yz} for different theories at two values of thermal conductivity parameter

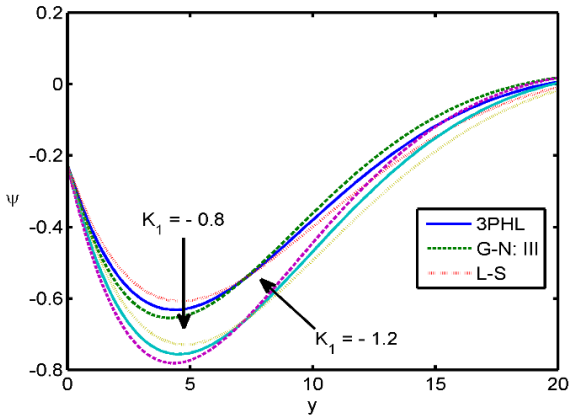

Fig. 22 The variation of the change in the volume fraction field ψ for different theories at two values of thermal conductivity parameter

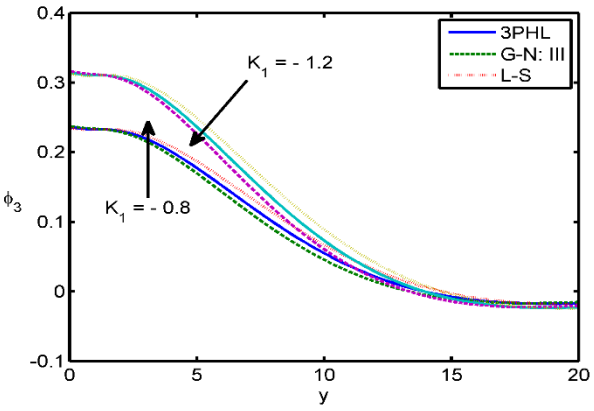

Fig. 23 The variation of the microrotation component ϕ_3 for different theories at two values of thermal conductivity parameter

against the distance y. We noticed from these figures that, the values of physical quantities at $K_1 = -0.8$ are larger

than the values of physical quantities at $K_1 = -1.2$. Figs. 20, 21 and 23 demonstrate the variation of the non-dimensional thermodynamic temperature θ, the couple stress tensor component m_{yz} and microrotation component ϕ_3, respectively. It is observed that: the values of variables at $K_1 = -0.8$ are smaller than the values of variables at $K_1 = -1.2$. It is observed that any small changes in the thermal conductivity lead to a considerable change in the propagation of wave behavior. Moreover the distinguishing curves of the physical quantities start from their initial values, and then begin to coincide, finally approaching zero value for large distance y.

8. Conclusions

The following points will help to conclude our present investigation:

- The theory of two-temperature generalized thermo-elasticity describes the behavior of the particles of the elastic body more real than the theory of one temperature generalized thermoelasticity.
- Theoretical as well as numerical results reveal that all the field variables are sensitive towards rotation and temperature discrepancy.
- The variable thermal conductivity and initial stress play a great role in our study, which have a significant effect on all fields.
- The continuous and impact loads have a good effect on all the physical fields.
- All figures display that the variations of all field quantities in the context of the 3PHL, G-N III and L-S theories of thermoelasticity follow similar trends.
- Deformation of a body depends on the nature of forced applied as well as the type of boundary conditions.
- The method used in the present article, Laplace-Fourier transforms technique, is applicable to a wide range of problems in thermodynamics.

Declaration of conflicting interests

The authors declared no potential conflicts of interest with respect to the research, authorship, and/or publication of this article.

Acknowledgments

The authors thank Taif University Researchers Supporting Project Number (TURSP-2020/230), Taif University, Taif, Saudi Arabia.

Funding

This research received funding from "Taif University Researchers Supporting Project Number (TURSP-2020/ 230), Taif University, Taif, Saudi Arabia".

Author contributions

The authors contributed equally to this work and approved it for publication.

References

Abbas, I.A. and Marin, M. (2018), "Analytical solutions of a two-dimensional generalized thermoelastic diffusions problem due to laser pulse", *Iran. J. Sci. and Tech. Trans. of Mech. Eng.*, **42**(1), 57-71. https://doi.org/10.1007/s40997-017-0077-1.

Barak, M.S. and Kaliraman, V. (2014), "Reflection and transmission of elastic waves from an imperfect boundary between micropolar elastic solid half space and fluid saturated porous solid half space", *Mech. Adv. Mater. Struct.*, **21**(9), 697-709. https://doi.org/10.1080/15376494.2018.1432795.

Belfield, A.J., Rogers, T.G. and Spencer, A.J.M. (1983), "Stress in elastic plates reinforced by fibre lying in concentric circles", *J. Mech. Phys. Solids*, **31**, 25-54.

Caputo, M. (1967), "Linear models of dissipation whose Q is almost frequency independent II", *Geophys. J. Int.*, **13**, 529-539. https://doi.org/10.1111/j.1365-246X.1967.tb02303.x.

Caputo, M. and Mainardi, F. (1971), "Linear model of dissipation in an elastic solids", *La Rivista del Nuovo Cimento*, **1**, 161-198. https://doi.org/10.1007/BF02820620.

Choudhuri, S.K.R. (2007), "On a thermoelastic three-phase-lag model", *J. Therm. Stress.*, 30, 231-238. https://doi.org/10.1080/01495730601130919

Eringen, A.C. and Suhubi, E.S. (1964), "Nonlinesr theory of simple micro-elastic solids-I", *Int. J. Eng. Sci.*, **2**(2), 189-203.

Eringen, A.C. (1966), "Linear theory of micropolar elasticity", *J. Appl. Math. Mech.*, **15**, 909-924.

Hobiny, A.D. and Abbas, I.A. (2020), "Fractional order thermo-elastic wave assessment in a two-dimensional medium with voids", *Geomech. Eng.*, 21(1), 85-93. https://doi.org/10.12989/gae.2020.21.1.085.

Khurana, A. and Tomar, S.K. (2019), "Waves at interface of dissimilar nonlocal micropolar elastic half-spaces", *Mech. Adv. Mater. Struct.*, **26**(10). https://doi.org/10.1080/15376494.2018.1430261.

Kumar, R. and Singh, B. (1996), "Wave propagation in a micro-polar generalized thermoelastic body with stretch", *Proc. Indian Acad. Sci.*, **106**(2), 183 199.

Kumar, R. and Rani, L. (2004), "Deformation due to mechanical and thermal sources in generalised orthorhombic thermoelastic material", *Sãdhanã*, **29**, 429-447.

Kumar, R. and Deswal, S. (2001), "Mechanical and thermal sources in a micropolar generalized thermoelastic medium", *J. Sound Vib.*, **239**(3), 467-488. https://doi.org/10.1006/jsvi.2000.3143.

Lata, P. and Zakhmi, H. (2019), "Fractional order thermo-elasticity study in orthotropic medium of type GN-III", *Geomech. Eng.*, **19**(4), 295-305. https://doi.org/10.12989/gae.2019.19.4.295.

Lata, P. and Kaur, H. (2020), "Effect of two temperature on isotropic modified couple stress thermoelastic medium with and without energy dissipation", *Geomech. Eng.*, **21**(5), 461-469. https://doi.org/10.12989/gae.2020.21.5.461.

Marin, M.,Othman, M.I.A., Seadawy, A.R. and Carstea, C. (2020), "A domain of influence in the Moore-Gibson-Thompson theory of dipolar bodies", *J. Taibah Univ. Sci.*, **14**(1), 653-660. https://doi.org/10.1080/16583655.2020.1763664.

Marin, M., Agarwal, R.P. and Mahmoud, S.R. (2013), "Modeling a microstretch thermo-elastic body with two temperatures", Abstract and Applied Analysis, 2013, Art. ID 583464, 1-7.

Marin, M. (2010), "A domain of influence theorem for microstretch elastic materials", *Nonlinear Anal.: R.W.A*., **11**(5), 3446-3452. https://doi.org/10.1016/j.nonrwa.2009.12.005.

Noda, N. (1986), "Thermal stresses in materials with temperature-dependent properties", Thermal Stresses I, (Ed., R.B. Hetnarski), North-Holland, Amsterdam.

Othman, M.I.A. and Singh, B. (2007), "The effect of rotation on generalized micropolar thermoelasticity for a half-space under five theories", *Int. J. Solid. Struct*., **44**(9), 2748-2762. https://doi.org/10.1016/j.ijsolstr.2006.08.016**.**

Othman, M.I.A. and Said, S.M. (2012), "The effect of rotation on two-dimensional problem of a fiber-reinforced thermoelastic with one relaxation time", *Int. J. Thermophys*., **33**, 160-171. https://doi.org/10.1007/s10765-011-1109-5.

Othman, M.I.A., Hasona, W.M. and Abd-Elaziz, E.M. (2014), "The effect of rotation on the problem of fiber-reinforced under generalized magneto-thermoelasticity subject to thermal loading due to laser pulse: A comparison of different theories", *Can. J. Phys*., **92**(9), 1002-1015. https://doi.org/10.1139/cjp-2013-0321.

Othman, M.I.A. and Song, Y.Q. (2009), "The effect of rotation on 2-D thermal shock problems for a generalized magneto-thermo-elasticity half-space under three theories", *Multi. Model. Mater. Struct*., 5(1), 43-58. https://doi.org/10.1108/15736105200900003.

Othman, M.I.A. and Said, S.M. (2019), "Effect of gravity field and moving internal heat source on a 2-D problem of a fiber-reinforced thermoelastic medium: Comparison of different theories", *Mech. Adv. Mater. Struct*., **26**(9), 796-804. https://doi.org/10.1080/15376494.2017.1410917.

Othman, M.I.A., Said, S.M. and Marin, M. (2019), "A novel model of plane waves of two-temperature fiber-reinforced thermoelastic medium under the effect of gravity with three-phase-lag model", *Int. J. Numer. Method. Heat Fluid Fl*., **29**(12), 4788-4806. https://doi.org/10.1108/HFF-04-2019-0359.

Parfitt, V.R. and Eringen, A.C. (1969), "Reflection of plane wavesfrom a flat boundary of a micropolar elastic half-space", *J. Acoust. Soc. Am*., **45**, 1258-1272

Roy, I., Acharya, D.P. and Acharya, S. (2017), "Propagation and reflection of plane waves in a rotating magneto elastic fibre-reinforced semi space with surface stress", *Mech. Mech. Eng*., **21**(4), 1043-1061.

Said, S.M. and Othman, M.I.A. (2015), "Influence of the mechanical force and the magnetic field on fiber-reinforced medium for three-phase-lag model", *Eur. J. Comp. Mech*., **24**(5) 210-231. http://dx.doi.org/10.1080/17797179.2015.1137751.

Said, S.M. and Othman, M.I.A. (2016), "Wave propagation in a two-temperature fiber-reinforced magneto-thermoelastic medium with three-phase-lag model", *Struct. Eng. Mech*., **57**(2), 201-220. http://doi.org/10.12989/sem.2016.57.2.201.

Said, S.M. and Othman, M.I.A. (2020), "The effect of gravity and hydrostatic initial stress with variable thermal conductivity on a magneto-fiber-reinforced", *Struct. Eng. Mech*., **74**(3), 425-434. https://doi.org/10.12989/sem.2020.74.3.001

Sarkar, N. and Atwa, S.Y. (2019), "Two-temperature problem of a fiber-reinforced thermoelastic medium with a model-I crack under Green-Naghdi theory", *Microsystem Technologies*, **25**, 1357-1367. https://doi.org/10.1007/s00542-018-4167-9.

Sarkar, N. and Lahiri, A. (2013), "The effect of gravity field on the plane waves in a fiber-reinforced two-temperature magneto-thermoelastic medium under Lord-Shulman theory", *J. Therm. Stress*., **36**, 895-914. https://doi.org/10.1080/01495739.2013.770709.

Sarkar, N. (2014), "Analysis of magneto-thermoelastic response in a fiber-reinforced elastic solid due to hydrostatic initial stress and gravity field", *J. Therm. Stress*., **37**(4), 387-404. https://doi.org/10.1080/01495739.2013.870845.

Sarkar, N. and Atwa, S.Y. (2019), "Two-temperature problem of a fiber-reinforced thermoelastic mediumwith a Mode-I crack under GreenNaghdi theory", *Microsys. Tech*., **25**(4), 1357-1367. https://doi.org/10.1007/s00542-018-4167-9.

Sarkar, N. and Modal, S. (2019), "Transient responses in a two-temperature thermoelastic infinite medium having cylindrical cavity due to moving heat source with memory-dependent derivative", *ZAMM*, **99**(6), e201800343. https://doi.org/10.1002/zamm.201800343.

Sarkar, N., Ghosh, D. and Lahiri, A. (2019), "A two-dimensional magneto-thermoelastic problem based on a new two-temperature generalized thermoelasticity model with memory-dependent derivative", *Mech. Adv. Mater. Struct*., **26**(11), 957-966. https://doi.org/10.1080/15376494.2018.1432784.

Sarkar, N. and Modal, S. (2020), "Two-dimensional problem of two-temperature generalized thermoelasticity using memory-dependent heat transfer: An integral transform approach"*, Ind. J. Phys.*, **94**, 1965-1974. https://doi.org/10.1007/s12648-019-01639-9.

Sengupta, P.R. and Nath, S. (2001), "Surface waves in fibre-reinforced anisotropic elastic media", *Sãdhanã*, 363-370.

Verma, P.D.S. and Rana, O.H. (1983), "Rotation of a circular cylindrical tube reinforced by fibers lying along helices", *Mech. Mater*., **2**(4), 353-359. https://doi.org/10.1016/0167-6636(83)90026-1.

Xue, B., Xu, H., Fu, Z. and Sun, Q. (2010), "Reflection and refraction of longitudinal displacement wave at interface between two micropolar elastic solid", *Adv. Mater. Res*., **139-141**, 214-217. https://doi.org/10.4028/www.scientific.net/AMR.139-141.214.

Zhang, P., Wei, P. and Tang, Q. (2015), "Reflection of micropolar elastic waves at the non-free surface of a micropolar elastic half-space", *Acta Mechanica*, **226**(9), 2925-2937. https://doi.org/10.1007/s00707-015-1346-y.

Zhang, P., Wei, P., and Li, Y. (2017), "Reflection of longitudinal displacement wave at the visco-elastically supported boundary of micropolar half-space", *Meccanica*, **52**(7), 1641-1654. https://doi.org/10.1007/s11012-016-0514-z.

JS

Appendix

$$B_1=\frac{A_1}{\rho c_1^2},\ B_2=\frac{A_2+\mu_L+\frac{P}{2}}{\rho c_1^2},\ B_3=\frac{\mu_L-\frac{P}{2}}{\rho c_1^2},\quad B_4=\frac{\beta_1}{\rho c_1^2},\quad B_5=\frac{k_1}{\rho c_1^2},$$

$$B_6=\frac{A_3}{\rho c_1^2},\ B_7=\frac{K c_1^2\eta}{K^*},\ B_8=\frac{\rho C_E n_0 c_1^2}{K^*},\ B_9=\frac{\rho C_E n_1}{\eta K^*},\quad B_{10}=\frac{\gamma^2 T_0 n_0 c_1^2}{K^* A_3},$$

$$B_{11}=\frac{\gamma^2 T_0 n_1}{\eta K^* A_3},\ B_{12}=\frac{\gamma m T_0 n_0 c_1^2}{K^* A_3},\quad B_{13}=\frac{\gamma m T_0 n_1}{\eta K^* A_3},\quad B_{14}=\frac{K_1}{c_1^2\eta^2\gamma_1},$$

$$B_{15}=\frac{2K_1}{c_1^2\eta^2\gamma_1},\ B_{16}=\frac{c_1^2 J\rho}{\gamma_1},\ B_{17}=\frac{\alpha_3}{c_1^2\eta^2\alpha_2},\ B_{18}=\frac{\alpha_4}{\eta\alpha_2},\ B_{19}=\frac{\alpha_5}{c_1^2\eta^2\alpha_2},$$

$$B_{20}=\frac{m A_3}{\alpha_2\gamma c_1^2\eta^2},\ B_{21}=\frac{c_1^2\rho\alpha_6}{\alpha_2},\qquad A_1=\lambda+2\alpha+4\mu_L-2\mu_T+\beta,$$

$$A_2=\lambda+\alpha,\ A_3=\lambda+2\mu_T,\ N_1=B_1\zeta^2+s^2-\Omega^2,\ N_2=B_3\zeta^2+s^2-\Omega^2,$$

$$N_3=\zeta^2+B_{15}+s^2B_{16},\ N_4=\zeta^2+B_{17}+B_{18}s+s^2B_{21},\ N_5=1+G_3+sB_7(1+G_4),$$

$$N_6=N_5\zeta^2,\qquad N_7=(1+G_1+G_2)(B_8s^2+B_9s),$$

$$N_8=(1+G_1+G_2)(B_{10}s^2+B_{11}s),\qquad N_9=\mathrm{i}\zeta N_8,$$

$$N_{10}=(1+G_1+G_2)(B_{12}s^2+B_{13}s),\quad N_{11}=1+\delta c_1^2\eta^2\zeta^2,\ N_{12}=\delta c_1^2\eta^2,$$

$$N_{13}=N_7N_{11}+N_6,\qquad N_{14}=N_7N_{12}+N_5,$$

$$G_1=\frac{\tau_q}{w_1}\left[\frac{qs+m}{s}(1-e^{-sw_1})-mw_1e^{-sw_1}\right],$$

$$G_2=\frac{s\tau_q^2}{2w_1}\left[\frac{qs+m}{s}(1-e^{-sw_1})-mw_1e^{-sw_1}\right],$$

$$G_3=\frac{\tau_T}{w_2}\left[\frac{qs+m}{s}(1-e^{-sw_2})-mw_2e^{-sw_2}\right],$$

$$G_3=\frac{\tau_T}{w_2}\left[\frac{qs+m}{s}(1-e^{-sw_2})-mw_2e^{-sw_2}\right],$$

$$G_4=\frac{\tau_\nu}{w_3}\left[\frac{qs+m}{s}(1-e^{-sw_3})-mw_3e^{-sw_3}\right],\qquad E_0=N_{38}N_{29}-N_{42}N_{16},$$

$$E_1=\frac{1}{E_0}(-N_{42}N_{40}+N_{16}N_{43}+N_{38}N_{45}-N_{39}N_{29}),$$

$$E_2=\frac{1}{E_0}(N_{42}N_{41}+2\Omega sN_3N_{30}+N_{40}N_{43}-2\Omega sN_{32}-N_{44}N_{16}-N_{38}N_{47}$$
$$-2\Omega sN_{46}-N_{39}N_{45}-2\Omega s\zeta^2N_{30}),$$

$$E_3=\frac{1}{E_0}(-N_{43}N_{41}-2\Omega sN_3N_{32}-N_{40}N_{44}-2\Omega sN_{34}+\mathrm{i}\zeta N_{28}N_{16}+N_{38}N_{49}$$
$$+2\Omega sN_{48}+N_{39}N_{47}-2\Omega s\zeta^2N_{46}),$$

$$E_4=\frac{1}{E_0}(N_{44}N_{41}+\mathrm{i}\zeta N_{28}N_{40}-N_{39}N_{49}+2\Omega s\zeta^2N_{48}),$$

$$E_5=\frac{1}{E_0}(-\mathrm{i}\zeta N_{28}N_{41}+2\Omega s\zeta^2N_3N_{34}),\qquad N_{15}=B_2\zeta^2-N_1,$$

$$N_{16}=\mathrm{i}\zeta(B_2-B_6),\quad N_{17}=N_1+B_3N_4,\qquad N_{18}=N_1N_4-B_4B_{19}\zeta^2,$$

$$N_{19}=\mathrm{i}\zeta(B_4B_{19}-B_2N_4),\qquad N_{20}=\mathrm{i}\zeta B_4B_{20}-N_4,$$

$$N_{21}=N_1N_{10}+\mathrm{i}\zeta B_4N_9,\qquad N_{22}=\mathrm{i}\zeta(B_2N_{10}-B_4N_8),$$

$$N_{23}=N_{11}N_{10}+N_{13}B_4,\qquad N_{24}=N_{12}N_{10}+N_{14}B_4,$$

$$N_{25}=B_3(N_{10}N_{12}-N_{24}),$$

$$N_{26}=N_{23}B_3+N_{17}N_{24}-N_{10}N_{11}B_3+N_{10}N_{12}N_{20}B_3-N_{12}N_{21},$$

$$N_{27}=-N_{17}N_{23}-N_{18}N_{24}-N_{10}N_{11}N_{20}B_3+N_{11}N_{21}-N_{12}N_{21}N_{20},$$

$$N_{28}=N_{18}N_{23}+N_{11}N_{20}N_{21},\qquad N_{29}=-\mathrm{i}\zeta B_2N_{24}+N_{22}N_{12},$$

$$N_{30}=2\Omega s(N_{10}N_{12}-N_{24}),\quad N_{31}=\mathrm{i}\zeta B_2N_{23}-N_{19}N_{24}-N_{11}N_{12}+N_{22}N_{12}N_{20},$$

$$N_{32}=2\Omega s(N_{23}+N_4N_{24}-N_{10}N_{11}+N_{10}N_{12}N_{20}),$$

$$N_{33}=N_{19}N_{23}-N_{11}N_{20}N_{22},\qquad N_{34}=2\Omega s(N_4N_{23}+N_{10}N_{11}N_{20}),$$

$$N_{35}=N_{10}N_{12}-N_{24},\qquad N_{36}=N_{23}+N_4N_{24}-N_{10}N_{11}+N_{10}N_{12}N_{20},$$

$$N_{37}=N_4N_{23}+N_{10}N_{11}N_{20},\quad N_{38}=\mathrm{i}\zeta B_3+N_{16},\quad N_{39}=\mathrm{i}\zeta(N_{15}+N_2),$$

$$N_{40}=\mathrm{i}\zeta(B_5B_{14}-N_2)+N_3N_{16},\qquad N_{41}=\mathrm{i}\zeta(N_2N_3-\zeta^2B_5B_{14}),$$

$$N_{42}=\mathrm{i}\zeta N_{25}+N_{29},\qquad N_{43}=\mathrm{i}\zeta N_{26}+N_{31},\qquad N_{44}=\mathrm{i}\zeta N_{27}+N_{33},$$

$$N_{45}=N_3N_{29}-N_{31}+\mathrm{i}\zeta B_5B_{14}N_{35},\qquad N_{46}=N_3N_{30}-N_{32},$$

$$N_{47}=N_3N_{31}-N_{33}+\mathrm{i}\zeta B_5B_{14}N_{36},\qquad N_{48}=N_{34}+N_3N_{32},$$

$$N_{49}=N_3N_{33}-\mathrm{i}\zeta B_5B_{14}N_{37},$$

$$H_{1n}=\frac{B_{14}(-N_{38}I_n^3+2\Omega sI_n^2-N_{39}I_n-2\Omega s\zeta^2)}{N_{16}I_n^4-2\Omega sI_n^3-N_{40}I_n^2+2\Omega sN_3I_n-N_{41}},$$

$$H_{2n}=\frac{(N_3-I_n^2)H_{1n}-B_{14}I_n}{\mathrm{i}\zeta B_{14}},$$

$$H_{3n}=\frac{B_3N_{10}I_n^2-N_{21}+(2\Omega sN_{10}-N_{22}I_n)H_{2n}-B_5N_{10}I_nH_{1n}}{\mathrm{i}\zeta(N_{23}-N_{24}I_n^2)},$$

$$H_{4n}=\frac{N_8I_nH_{2n}-N_9+(N_{14}I_n^2-N_{13})H_{3n}}{N_{10}},\qquad H_{5n}=(N_{11}-N_{12}I_n^2)H_{3n},$$

$$H_{6n}=\frac{1}{A_1}(\mathrm{i}\zeta A_2-A_3I_nH_{2n}+\beta_1H_{4n}-A_1H_{5n}),$$

$$H_{7n}=\frac{1}{A_1}[\mathrm{i}\zeta(\mu_L-\frac{P}{2})H_{2n}-(\mu_L+\frac{P}{2})I_n-k_1H_{1n}],$$

$$H_{8n}=-\frac{\eta^2\gamma_1}{\rho}I_nH_{1n}.$$